

## Hot-electron-driven charge transfer processes on O<sub>2</sub>/Pt(111) surface probed by ultrafast extreme-ultraviolet pulses

C. Lei,<sup>1,\*</sup> M. Bauer,<sup>2</sup> K. Read,<sup>1</sup> R. Tobey,<sup>1</sup> Y. Liu,<sup>3</sup> T. Popmintchev,<sup>1</sup> M. M. Murnane,<sup>1</sup> and H. C. Kapteyn<sup>1</sup>

<sup>1</sup>JILA, University of Colorado, Boulder, Colorado 80309-0440

<sup>2</sup>Fachbereich Physik, University Kaiserslautern, D-67663 Kaiserslautern, Germany

<sup>3</sup>Center for X-ray Optics, Lawrence Berkeley National Laboratory, Berkeley, California 94720

(Received 20 June 2002; revised manuscript received 18 September 2002; published 31 December 2002)

We use ultrafast extreme-ultraviolet photoelectron spectroscopy to directly monitor the electron dynamics and the characteristic valence-band photoelectron spectra associated with a hot-electron mediated surface chemical reaction. By adsorbing molecular oxygen onto a Pt(111) surface and exciting it with an ultrafast laser pulse, charge transfer induced changes in the platinum-oxygen bond were observed on femtosecond time scales. By simultaneously monitoring both the hot-electron distribution at the Fermi edge and the valence-band photoemission spectra, it was determined that the thermalization of the hot-electron gas precedes significant changes in the O<sub>2</sub>/Pt bond.

DOI: 10.1103/PhysRevB.66.245420

PACS number(s): 82.53.St, 68.43.-h, 68.35.Ja, 79.60.-i

### I. INTRODUCTION

The study of ultrafast processes on surfaces has been a topic of increasing interest in recent years.<sup>1</sup> Two considerations motivate this interest. First, ultrafast (picosecond and femtosecond) times correspond to the fundamental time scale for atomic motion in a surface reaction.<sup>2</sup> And second, progress in the development of ultrafast light sources<sup>3</sup> has recently made possible different types of investigations. These interesting experiments, in conjunction with molecular modeling,<sup>4,5</sup> have the potential to bring our understanding of surface science to a new level of sophistication, yielding new insights into mechanisms as well as providing important confirmation of current models and simulation. Such a detailed understanding of surface reaction dynamics is especially important to processes such as heterogeneous catalysis, where the interaction between the molecule and the surface itself is fundamental to the process.

Observing a dynamic process on a surface is experimentally challenging. In the case of gas and solution phase chemistry for example, pump-probe transient absorption spectroscopy and numerous more sophisticated techniques have been used to obtain a clear picture of reaction dynamics.<sup>6</sup> Unfortunately, on a surface the very small (monolayer) sample size makes transient-absorption studies impossible. Nevertheless, past time-resolved surface studies have used a number of techniques such as two-photon photoemission, IR spectroscopy, sum-frequency generation, and resonant Auger spectroscopy to monitor phonon and electron substrate-adsorbate coupling on ultrafast time scales.<sup>7-10</sup> This work has already yielded different insights; however, current experiments have been very limited in their ability to obtain direct, time-resolved, information on the process most central to surface chemistry: the making and breaking of chemical bonds.

In the case of non-time-resolved studies of surface processes, photoemission spectroscopy has proven to be one of the most useful experimental tools.<sup>11</sup> It is extremely sensitive and inherently surface specific because of the short escape depths of the emitted photoelectrons. In valence-band ultra-

violet photoemission (UPS), photons with energy  $\geq 10$  eV are used to provide direct information on the electrons involved in the chemical bond; for example, the hybridization of the outermost molecular orbitals responsible for the bond.<sup>12,11</sup> In core-level x-ray photoelectron spectroscopy (XPS), higher energy soft x rays are used to observe the “chemical shift” of a core level.<sup>13</sup> Since these core levels are specific to particular atoms, XPS gives site specific information about atoms in different chemical environments.

Most previous UPS/XPS studies have used x-ray sources incapable of providing time-resolved information. In contrast, time-resolved photoemission studies have been limited by the difficulty of obtaining ultrafast pulses in the UV and x-ray regions of the spectrum. For example, in recent work using two-photon photoemission, Petek *et al.* observed the motion of a cesium atom on a surface.<sup>8</sup> By exciting the Cs atom to a relatively long-lived (= 100 fs) electronically excited state, it was possible to then photoeject this excited-state electron to observe the atomic motion. However, this experiment used an ultrafast laser source with a photon energy insufficient to eject electrons from the ground state. Since the electronic ground state could not be directly observed, this experiment was limited by the lifetime of the probed excited state in its ability to follow the entire process. Other UV photoemission experiments have studied the dynamics of “image potential state” electrons at surfaces, however, here the atomic structure of the surface was static.<sup>14</sup>

Recent progress in the generation of ultrafast light pulses at short wavelengths now makes femtosecond resolution UPS/XPS experiments feasible. During the past several years, ultrafast x rays generated through the process of high harmonic generation (HHG) have been used in both non-time-resolved core-level photoelectron spectroscopy studies, and for observing the decay dynamics of photoexcited electrons at a surface and in thin films.<sup>15</sup> In high harmonic generation, an ultrafast laser pulse focused into an atomic gas generates harmonics of the driving field frequency that extend into the soft x-ray region of the spectrum. The recent development of a phase-matched waveguide geometry for HHG has made it possible to generate fully coherent, high-flux ( $> 10^{12}$  photons/sec), beams of extreme ultraviolet

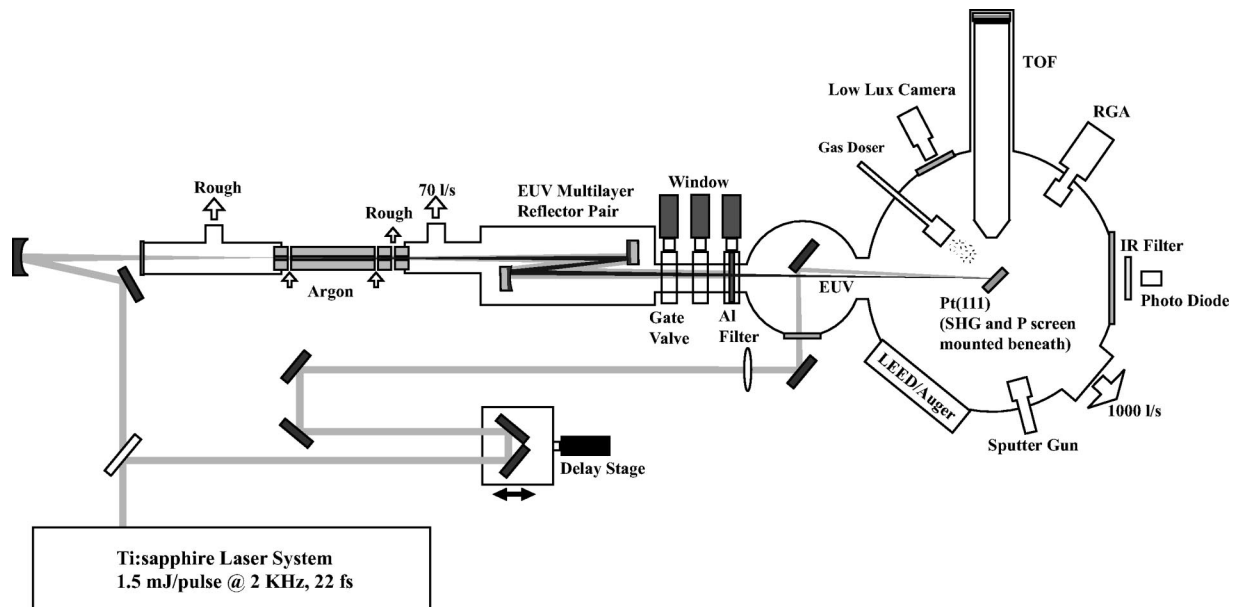


FIG. 1. Schematic diagram of the experimental setup for femtosecond time-resolved valence-band spectroscopy using EUV light.

(EUV) light using a very simple and practical geometry.<sup>16</sup>

In past work, we used these advances in EUV sources to perform direct observation of changes in the bonding of a molecule on a surface as result of an ultrafast charge-transfer process.<sup>17</sup> An ultrafast laser pulse at 800 nm was used to irradiate a Pt(111) surface coated with a monolayer of O<sub>2</sub>. After transient heating of the surface by the laser pulse, an ultrashort-pulse (5 fs) EUV beam at 42 eV was used to monitor changes in the valence-band structure of the Pt/O<sub>2</sub> complex. This enabled us to observe subpicosecond time-scale changes in the chemical bond character on a surface, and to observe the molecular dynamics over an extended period ( $\sim 10$  ps) from start to the finish of the reaction.

In this paper, we use time-resolved extreme ultraviolet photoemission spectroscopy (TR-UPS) to follow simultaneously different steps of a surface chemical reaction. We monitor the time evolution of the hot, nonequilibrium, electron distribution after excitation by an ultrashort optical excitation pulse. In addition, changes in the valence band of the O<sub>2</sub>/Pt(111) are observed, indicating a reversible adsorbate state transition driven by an electron transfer from the surface to the adsorbate. Simple models are also used to predict the electron and phonon temperatures as a function of time. We find that the hot, nonequilibrium, electron distribution thermalizes before there is any change in the characteristic photoemission spectrum of the O<sub>2</sub>/Pt complex, i.e., before there is time for the bond or local environment of the O<sub>2</sub> to change as a result of the charge transfer.

## II. EXPERIMENTAL SETUP

Figure 1 shows a schematic diagram of our experimental setup. A platinum (111) single crystal is mounted inside an ultrahigh vacuum (UHV) chamber with a base pressure of less than  $1 \times 10^{-10}$  torr. The sample is spot welded onto tantalum wires and attached to a manipulator with temperature

control capability. The sample is frequently cleaned by standard platinum surface cleaning procedures: 800-eV argon ion sputtering for 10 min, 650° C oxygen annealing treatment for 10 min, and subsequent annealing of the platinum crystal to 1000° C for one min at a background pressure below  $10^{-9}$  torr. The UHV chamber is also equipped with LEED (low-energy electron diffraction) and AES (auger electron spectroscopy) probes, and a TDS (thermal desorption spectroscopy) analyzer; the surface condition can thus be easily monitored. The femtosecond pulses are generated by an amplified Ti:sapphire laser system that generates 1.5-mJ pulses with a duration of less than 22 fs, and at a repetition rate of 2 kHz. The laser beam is first split using a beam splitter to generate the pump and probe beams. The relative time delay between these beams is adjusted using a computer-controlled translation stage. The 800-nm pump beam, broadened to 55 fs due to dispersion in the beam splitter and other optics, is gently focused onto the sample at 45° at an absorbed fluence of up to 4 mJ/cm<sup>2</sup> (*p* polarized). The fluence is adjustable using a half wave plate and a polarizer. The absorbed fluence is calculated from the incident fluence at the sample and values of the dielectric function of Pt from the literature.<sup>18</sup> The 800-nm probe beam is upconverted to EUV light using phased matched high harmonic generation in a hollow fiber. This process generates a coherent, low-divergence, EUV beam, consisting of three to five harmonics (= orders 25–31), and with a pulse duration of less than 10 fs. Details of the fiber cell can be found in Ref. 16. A set of two multilayer mirrors are installed after the exit of the fiber at normal incidence. The wavelength selectivity of the multilayer mirror serves to select only a single harmonic order (27th at 42 eV) to excite the Pt sample. The polarization can be selected as *p* or *s*, depending on the polarization of the driving IR pulses. The resultant reflectivity curve for the multilayer mirror pair is shown in Fig. 2. Because the total thickness in reflection of the multilayer mirror stack is only

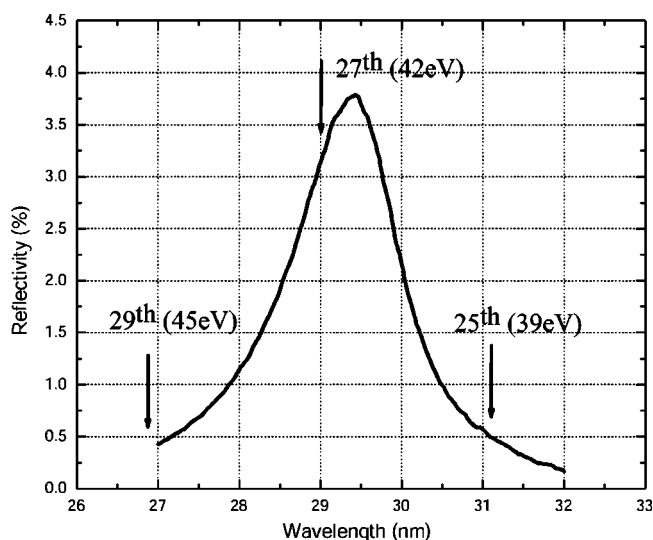


FIG. 2. Total reflectivity curve of the multilayer mirror pair.

320 nm/mirror (corresponding to  $\sim 2$  fs round trip), and because simple quarter-wave multilayer mirror optics generally do not result in pulse broadening, the reflected EUV pulse will not be temporally broadened. Thus, in contrast to systems that use a diffraction grating,<sup>19</sup> this setup allows selection of a single harmonic order without temporal broadening. In addition, the second curved multilayer mirror is used to focus the EUV beam to a spot size of  $400 \mu\text{m}$  on the Pt sample. An aluminum filter ( $0.2 \mu\text{m}$  thick) between the sample and the multilayer mirror pair blocks the infrared beam while transmitting the EUV beam. The total dispersive broadening induced by aluminum filter and the multilayer mirrors is estimated to be less than 1 fs. The small relative angle ( $< 1^\circ$ ) of incidence between the pump and probe beams limits the geometrical degradation in time to below 2 fs. The kinetic energy of the photoemitted electrons is measured using a time-of-flight (TOF) detector with a 60-cm tube length and 40-mm-diameter active area. The solid angle at collection is  $10^{-2}$  steradians. The detector energy resolution is limited by the 0.8-ns “delta-function” time response of the data acquisition system, determined from the width of the “time zero” peak that results from EUV light scattered from the surface. The resolution can be estimated by the temporal width of the EUV photons scattered from the surface, which results in a 0.3-ns-wide FWHM peak.

To find the temporal and spatial overlap between the pump and probe beams, a phosphor screen and a second harmonic crystal (SHG) are mounted beneath the sample and can be placed in the beam by repositioning the manipulator. The phosphor screen allows us to observe an image of the EUV beam using a charge-coupled device (CCD) camera, and to overlap the pump and probe beams spatially. To find the temporal overlap, a second harmonic crystal is moved to the same position as the sample. The infrared 800-nm light used to generate the EUV beam is allowed into the UHV chamber by replacing the Al filter with a thin ( $355 \mu\text{m}$ ) sapphire window. By performing a cross correlation between the pump and probe beams, the time zero for the experiment can be accurately identified, as shown in Fig. 3(a). The

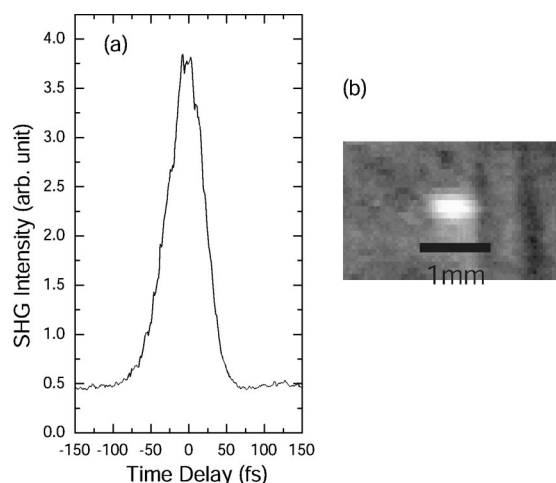


FIG. 3. (a) Second harmonic signal generated by cross correlating the infrared pump and probe beams. The FWHM is 62 fs. (b) Image of the EUV beam on a phosphor screen at the position of the Pt sample. The spot size is  $400 \mu\text{m}$ .

934-fs extra time delay induced by the sapphire window on the probe beam can be corrected by moving the translation stage on the pump beam. The full width at half maximum (FWHM) of the second harmonic signal is 62 fs. The 62-fs resolution represents an upper limit for the resolution, given that the EUV pulse duration is shorter than that of the driving laser and should be  $\leq 10$  fs.

### III. EXPERIMENTAL RESULTS

Due to its simplicity and relevance to catalytic reactions, the  $\text{O}_2/\text{Pt}(111)$  system has been investigated both experimentally and theoretically in considerable detail. Five different adsorption states of oxygen on Pt(111) have been reported to date: Molecular oxygen can be found in one physisorbed ( $T \leq 30$  K) and three different chemisorbed states (at  $T \leq 145$  K). The preferred configuration of chemisorbed  $\text{O}_2$  at saturation coverage is in a superoxo state occupying a bridge site ( $\text{O}_2^-$ ). At low coverages it is predominantly found in the peroxo configuration ( $\text{O}_2^{2-}$ ) at a threefold hollow site [see Fig. 4(a)]. A third configuration has been identified as result of step site adsorption. At elevated temperatures above 145 K, dissociative adsorption is also observed.<sup>20–25</sup> Comparing spectra of a clean Pt(111) surface and a Pt(111) surface covered with a saturation layer of molecular oxygen at liquid-nitrogen temperature (superoxo oxygen), photoemission signal from the Pt  $d$  bands of the latter case is strongly reduced due to adsorption of oxygen. At the low-energy side of the valence band, at binding energies, referenced to the Fermi level, of about 6 eV, an oxygen-related feature appears in the spectra. This feature has been observed previously using synchrotron sources, and has been assigned to the occupied oxygen  $1\pi_g^*$  orbitals of the free molecule,<sup>26</sup> in agreement with results from density-functional theory calculations.<sup>27,28</sup> We found that, at the photon energy of 42 eV used, this feature is particularly sensitive to the chemical bond character of the oxygen. Figure 4(b) shows the low-energy part of the valence spectra for different

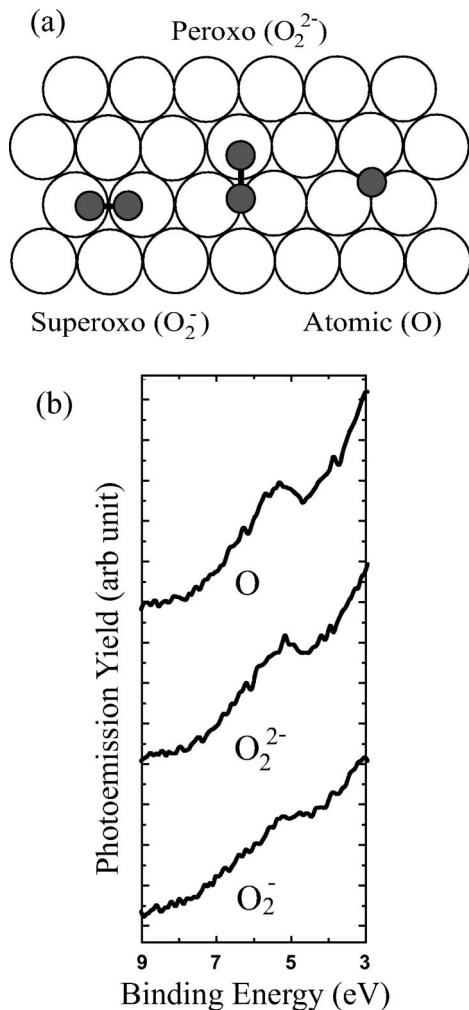


FIG. 4. (a) Schematic diagram of the surface configuration of oxygen on Pt(111), for the superoxo ( $O_2^-$ ), peroxo ( $O_2^{2-}$ ), and atomic (O) states. (b) Static photoemission spectra taken for the superoxo ( $O_2^-$ ), peroxo ( $O_2^{2-}$ ), and atomic (O) states.

chemical modifications of oxygen on Pt(111). The bottom curve corresponds to the superoxo configuration (high coverage). By heating the surface to 138 K, a partial desorption of molecular oxygen (see Fig. 5) increases the occupation of peroxo adsorption sites with respect to the superoxo configuration.<sup>24</sup> The corresponding photoemission spectrum is shown in the middle curve. The top curve shows the characteristic spectrum for the atomic oxygen adsorption state. In qualitative agreement with results by Puglia and co-workers, we observe a change in the spectral shape of the  $1\pi_g^*$  orbital between the superoxo and peroxo states, but no significant difference in this energy region between the peroxo oxygen and the atomic oxygen states. The different adsorption states can also be distinguished by means of thermal desorption spectroscopy (see Fig. 5). Two distinct desorption peaks can be observed for this system: An intense  $\alpha$ - $O_2$  peak at 145 K due to desorption of molecularly bonded oxygen, and a weaker high-temperature  $\beta$ - $O_2$  peak as result of recombinative desorption of atomic oxygen. The very different desorption temperatures mean that the molecular state has a much lower binding energy than the atomic state. The molecular

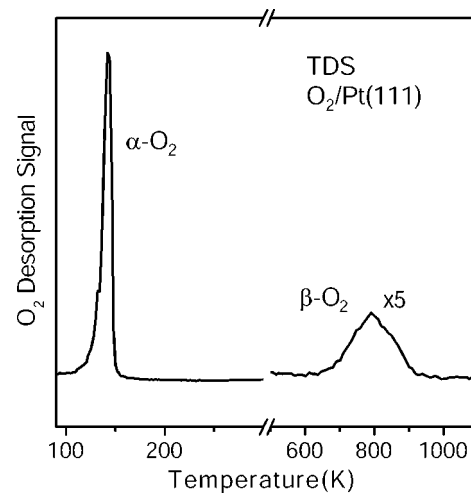


FIG. 5. Thermal desorption spectrum (TDS) for Pt(111) covered with  $O_2$ : the rate of temperature increase is 3 K/sec from 77 to 300 K; then 10 K/sec from 300 to 1100 K.

state likely resides in a different adsorption site, and has a different bonding character than the atomic state. Before the TDS heating cycle starts, only molecular oxygen is adsorbed on the surface—the atomic oxygen is solely a result of dissociation of the molecular oxygen. This progresses by means of peroxo excitation; the peroxo oxygen state is therefore sometimes referred to as the “intermediate” or “precursor” state of dissociated atomic oxygen.

Interaction of intense femtosecond laser pulses with  $O_2$ /Pt(111) has been studied in the past using photodesorption yield measurements.<sup>25,29</sup> In particular, a nonlinear dependence of desorption yield on intensity was reported. This behavior has been reported for a variety of adsorption systems, and has been proposed to be the result of a direct coupling between the excited hot-electron gas and the oxygen molecules, without involvement of the substrate lattice (phonons).<sup>5</sup> This work has also identified another nonspecific reaction channel for the adsorbed oxygen, resulting in a configuration that hinders re-adsorption of oxygen back onto the platinum surface.<sup>30</sup> Therefore subsequent laser-induced desorption and deposition cycles result in a decreasing desorption yield. Figure 6 shows femtosecond-induced desorption yield traces for two subsequent cycles. This observation indicates that a surface modification other than depletion takes place, resulting in a diminished number of free adsorption sites in subsequent cycles. For the present time-resolved (pump-probe) photoemission experiments, it is necessary to quench both of these (obviously nonreversible) processes. In all cases for our experiment, we used a low ( $1 \text{ mJ/cm}^2$ ) pump fluence to keep desorption negligible. From extrapolation from reference data<sup>29</sup> we estimate that at this fluence, significant desorption requires more than an hour. However, as will be shown later, on longer time scales a permanent modification of the sample state (either through depletion, or by means of another reaction channel) is observed in our spectra.

For the time-resolved pump probe photoemission experiment, a saturation layer of molecular oxygen was adsorbed onto the Pt surface at liquid-nitrogen temperature. Photo-

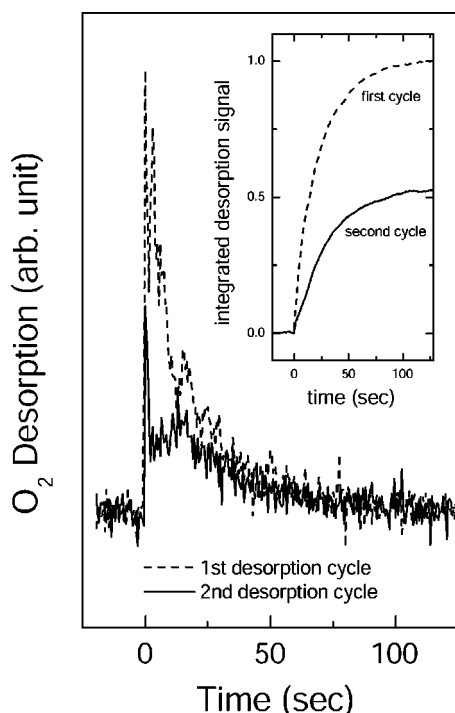


FIG. 6. Femtosecond laser-induced desorption for first and second desorption cycles. The inset shows the integrated desorption signal for the two cycles.

emission spectra at different temporal delays between the excitation (pump) pulse and the UV probe pulse were then taken. We observe significant changes in the spectrum as function of temporal delay between pump and probe in two different energy regions: at the Fermi edge, and at a binding energy of 6 eV where the oxygen-induced feature ( $1\pi_g^*$ ) appears. Figure 7 shows the transient modifications at the Fermi edge observed at different delays. At time zero (i.e., when pump and probe arrive temporally coincident at the surface) the shape of the Fermi edge is modified by a “step” at energies above the Fermi edge with a width of about 1.5 eV, corresponding to the energy of the exciting photons. Some evidence of this feature is still visible at 150 fs delay. Within another 100 fs, 250 fs after the pump, this nonthermal contribution has completely disappeared. At longer delays, no further changes in this energy region can be observed. The experimental distribution at time zero is best reproduced by an excitation level of about 6% (at a photon energy of 1.5 eV). Referring to the solid curve in inset of Fig. 7, the solid line is the calculated distribution for this case, convolved with the detector resolution of 370 meV. For reference, a spectra taken without the pump beam (ground-state distribution) is fit to a Fermi-Dirac distribution at 100 K, also convolved with the detector resolution.

Figure 8 shows a pump probe scan of the low-energy part of the valence-band spectra. For reference, a photoelectron spectrum without pump beam present was taken initially, as shown in Fig. 8(a). The shoulder corresponds again to the superoxo oxygen  $1\pi_g^*$  level at 6 eV binding energy as described above. Figure 8(b) shows the spectrum obtained with the probe coincident in time with the pump beam (i.e., time

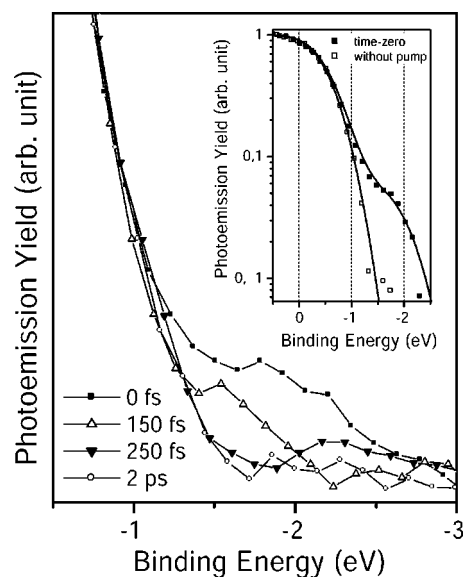


FIG. 7. Electron energy distribution at Fermi edge of  $O_2/Pt(111)$ , for time delays of 0, 150, and 250 fs, and 2 ps. Non-equilibrium hot electrons can be seen at 0 and 150 fs, however, at 250 fs, the energy distribution has thermalized. Inset: Fermi edges at 0 fs time delay (black square) and static spectrum without pump pulses excitation (hollow square), plotted in log scale. The electron distribution at 0 fs time delay can be fit to a 100-K Fermi-Dirac distribution with 6% of the electrons excited by the pump photon energy (1.5 eV).

zero). In contrast to the Fermi edge, where at zero time delay the most obvious change compared to the ground state was observed, no significant changes are visible compared to the static spectrum. However, 250 fs later—well after the 55-fs pump pulse has been absorbed and the nonthermal distribution at the Fermi edge has disappeared—a new peak has appeared. This peak is even stronger at a pump-probe delay of 500 fs, and persists for several ps. Since our experimental approach involves sequential pump-probe scans, we confirmed that this feature is not due to a permanent change of the sample, by taking a spectrum at zero time delay immediately after the 500-fs scan. This spectrum is identical to spectra (a) and (b). Thus, in this experiment, the observed changes are reversible, indicating that a transient modification of the adsorbate bonding is monitored in this experiment. From more detailed scans we are able to extract characteristic population and relaxation rates of this transient (metastable) excited adsorbate state. Figure 8(f) shows a plot of the integrated strength of this transient peak, as a function of time delay. The observed peak has an exponential onset of  $550 \pm 140$  fs, and decays within about 5 ps.

In addition to this reversible change in the valence-band structure, over time scales of hours we also observe a long-term nonreversible change of the surface state induced by the IR-pump pulse. Figure 9 shows a series of spectra taken during a period of 2 h of irradiation by the IR pump pulse. During the first hour of IR irradiation following dosing of the Pt by oxygen, no significant changes in the spectrum are observed. However, further IR-irradiation alters the shape of the 6-eV feature into a peaklike structure, as observed before

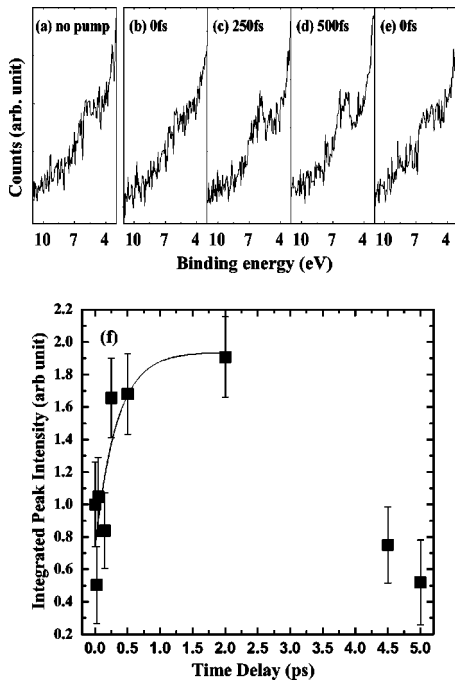


FIG. 8. Time-resolved high-resolution photoemission spectra from a saturation layer of molecular oxygen adsorbed on a Pt(111) surface at liquid-nitrogen temperature: (a) no pump beam; (b) with pump beam, zero delay between pump and probe; (c) 250 fs delay between pump and probe; (d) 500 fs delay; (e) repeat of (b), taken immediately after (d); (f) integrated amplitude of the characteristic 6-eV peak feature as a function of pump-probe delay. A fit to the data indicates an onset time of  $550 \pm 140$  fs (from Ref. 17).

for the atomic and peroxy state of oxygen as well as in the transient state spectra. On longer time scales this feature in the photoelectron spectrum seems to represent the stabilized configuration of the surface, and does not alter with further IR irradiation.

#### IV. DISCUSSION

The progression of the surface chemical reaction induced by the intense pump pulse is as follows: (i) creation of a

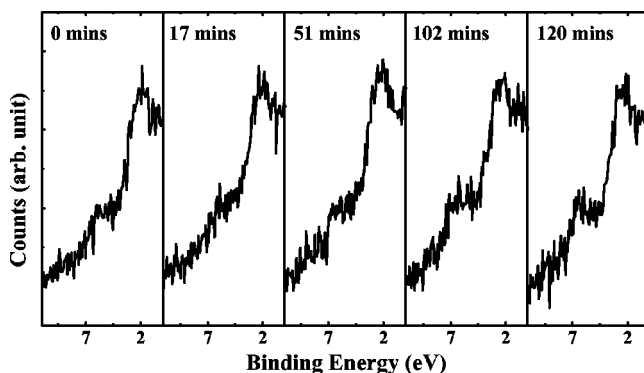


FIG. 9. Spectra taken during pump beam irradiation of the sample over a period of 2 h. During the first  $\approx 50$  min, the spectra are unchanged. However, after  $\approx 100$  min the characteristic 6-eV peak gradually increases and is permanently present on the sample.

nonthermal electron distribution in the substrate due to absorption of the ultrashort laser pulse, (ii) internal thermalization of the excited electron gas, and adsorbate excitation due to electron-mediated energy transfer, (iii) a modification of the chemical bonding character, resulting in adsorbate motion, (iv) thermalization between the electron gas and the phonon gas, and (v) traditional “phonon induced” chemical surface reaction due to elevated lattice temperature that happens in a much longer time scale. We relate the transient modifications of the photoelectron spectra observed in our experiment to processes corresponding to steps (i) and (iii). Knowledge of the absorbed fluence as well as the measured excitation rate of the electron gas allows us to reconstruct step (ii) as well as step (iv). Our analysis is discussed in detail as follows.

Due to the low optical density of the adsorbate layer, the energy of the incident laser pulse is absorbed entirely in the free-electron gas of the Pt(111). On femtosecond time scales, this results in an extremely nonthermal distribution of the electron gas, as is observed at time-zero as a step at the Fermi edge. The absorbed fluence of  $1 \text{ mJ/cm}^2$  results in an excitation of about 6% of the electrons at the surface. The 42-eV probe pulse photons eject electrons from the top  $5 \text{ \AA}$  of the platinum.<sup>31</sup> Comparable excitation levels have been reported for heating a  $300 \text{ \AA}$  thick gold film and a Pt(110)-oriented surface.<sup>32,33</sup> The detected nonthermal character of the electron distribution disappears within the first 250 fs, in agreement with the results for Pt(110). In contrast, significantly longer lifetimes of the nonthermal contribution (up to 400 fs) have been reported for gold. This difference can be related to a much slower electron thermalization process in noble metals in comparison to transition metals, due to a reduced electron-electron scattering rate at the relevant energies.<sup>34,35</sup> It is a direct consequence of the reduced density of electron states at the Fermi edge for noble metals.

Knowledge of the absorbed fluence allows us to calculate the time evolution of the electron and lattice temperatures. Due to its low heat capacity, the electron gas is heated quite efficiently by the laser pulse. Although the nonthermal character of the electron distribution immediately after excitation does not allow us to assign a simple temperature to the system, the calculated electron energy distribution is a useful indicator of the actual excitation state. Thermalization of the electron distribution occurs in  $\sim 250$  fs, followed by subsequent cool-down of the electron gas due to coupling to the lattice (electron-phonon coupling) and thermal conduction into the bulk. The electron-phonon effective collision time is actually of the same order as the electron-electron scattering time; however, it is quite inefficient with respect to collisional energy exchange (of the order of typical phonon energies, some tens of meV). Thus excitation of the lattice occurs on much longer time scales than the electron dynamics. In addition, the higher heat capacity of the lattice limits the maximum lattice temperature to much lower temperatures. The interaction of laser, electron gas, and lattice (phonon gas) can be modeled using a set of coupled equations that determine the electron ( $T_e$ ) and lattice ( $T_p$ ) temperatures as a function of time,<sup>36</sup>

TABLE I. Parameters of platinum (111) used in the calculation of electron and lattice temperatures.

Electron specific heat $\gamma$	748 J/m <sup>3</sup> K <sup>2</sup>
Thermal conductivity $\kappa_0$ (77 K)	71.6 W/m K
Electron-phonon coupling constant $g$	$6.76 \times 10^{17}$ W/m <sup>3</sup> K
Lattice heat capacity $C_p$ (77 K)	$2.69 \times 10^6$ J/m <sup>3</sup> K
Absorbed laser peak intensity $I_0$	$1.71 \times 10^{14}$ W/m <sup>2</sup>
Pulse width $\tau$	55 fs
Optical penetration depth $\lambda$ (800 nm)	12.56 nm

$$C_e \frac{\partial}{\partial t} T_e = \frac{\partial}{\partial z} \left( \kappa \frac{\partial}{\partial z} T_e \right) - g(T_e - T_p) + \hat{F}, \quad (1)$$

$$C_p \frac{\partial}{\partial t} T_p = g(T_e - T_p), \quad (2)$$

where  $C_e = \gamma T_e$  and  $C_p$  are the electron and lattice heat capacities, respectively.  $\kappa = \kappa_0(T_e/T_p)$  is the thermal conductivity and  $g$  is the electron-phonon coupling constant. The term  $\hat{F}$  is used to describe the femtosecond pump pulse in the form of

$$\hat{F} = \frac{I_0}{\lambda} e^{-4 \ln(2)t/\tau - z/\lambda}, \quad (3)$$

where  $I_0$  is the absorbed laser peak intensity,  $\lambda$  is the optical penetration depth, and  $\tau$  is the pump pulse width. All the parameters used in this simulation are listed in Table I

For a platinum surface excited by a 1-mJ/cm<sup>2</sup> laser fluence, we predict a peak electron temperature of 1082 K, 35 fs after time zero [immediately after the laser pulse (55 fs) has ended] [Fig. 10(a)]. The same value for the maximum temperature (about 1000 K) can be calculated from the measured excitation of the electron gas of 6%.<sup>37</sup> In contrast, the calculated maximum temperature of the lattice, 174 K, is reached 1.2 ps after excitation. At this point, the electron and lattice temperatures are equilibrated. Figure 10(a) shows that at long delays, the lattice temperature is higher than the electron temperature. This is because only electron heat diffusion

is considered in Eq. (1), due to the fact that lattice heat diffusion is much slower than electron heat diffusion. At this point, the surface temperature is still much higher than the bulk temperature, so that the electrons keep diffusing energy into the bulk while the lattice only gives up energy to the electrons. True equilibrium happens at very long delays, when the surface and bulk temperatures are similar. Note that a change in the slope of the Fermi-dirac distribution in the experimental data, which would reflect the heating of the electron gas, is not visible. In contrast to the transient non-thermal distribution, which clearly shows up in our experiment, the energy resolution of our detector, together with the limited statistics of the measurement does not as yet allow us to observe these thermal effects.

Figure 10(b) compares the integrated intensity of the characteristic peroxy peak to the electron and lattice temperature. The oxygen peak is delayed about 1 ps with respect to the time when the peak electron temperature is reached; thus, the electrons have largely cooled before the oxygen peak relaxes. On the other hand, the lattice temperature has a rise time similar to the oxygen peak, but the lattice temperature cools on very long time scales compared with the relaxation time of the oxygen peak. If the observed oxygen transient were driven primarily by lattice excitation, the relaxation time of the oxygen peak would be much longer than observed—comparable to the lattice relaxation time. Furthermore, a finite time delay between the maximum oxygen peak and the time of the peak lattice temperature would probably also be expected, given the finite coupling time of excitation into the adsorbates. Therefore the hot electrons are likely to be directly driving the changes in the oxygen configuration, while they are simultaneously losing energy to the lattice.

It is useful to compare the time scales of the different thermalization processes with the appearance of the transient changes in the  $1\pi_g^*$  orbital of the oxygen. These changes reflect a transient change of the chemical state of the molecule resulting from coupling to the excited electron gas. The lifetime of this state significantly exceeds the cooldown time of the hot-electron gas, by 5 ps the electron gas has cooled and transferred its energy to the lattice. Furthermore, it is noteworthy that the  $1\pi_g^*$  orbital is quite important with re-

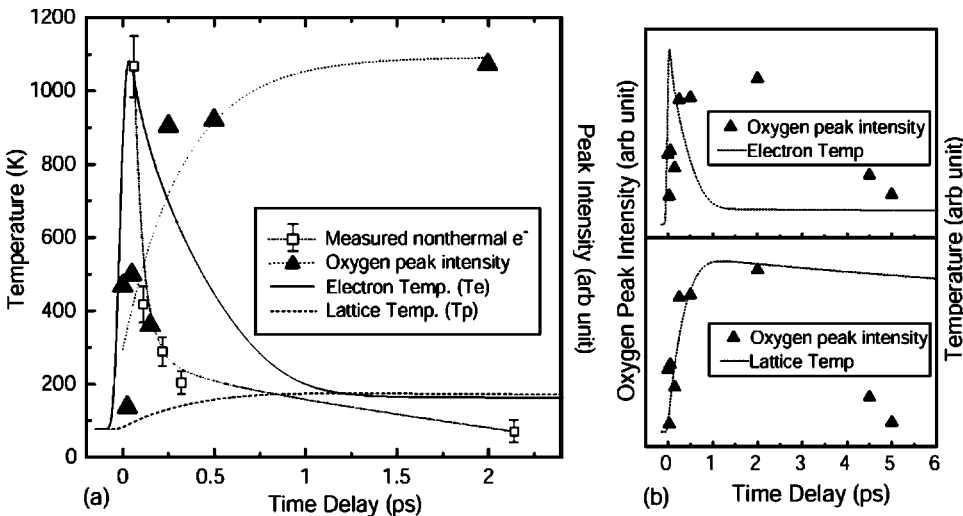


FIG. 10. (a) Calculations of electron ( $T_e$ ) and lattice ( $T_p$ ) temperatures for  $10\text{-}\mu\text{J}/\text{mm}^2$ , 55-fs, pump pulse excitation. The measured nonthermal electron distribution and the integrated intensity of the peroxy signature peak are also shown for comparison. (b) Integrated intensity of the peroxy signature peak compared to the rescaled electron and lattice temperature.

spect to the interaction between molecular oxygen and the platinum surface: On the one hand it is antibonding with respect to the intramolecular O-O bond; on the other hand hybridization of this state with platinum *d* states results in an effective bond between the Pt surface and oxygen. Spectral changes thus reflect changes in the oxygen bond length as well as the molecule surface interaction. This is exactly what we observe for the static spectra when comparing different chemical states of the oxygen. Transformation from the superoxo into the peroxy state of oxygen accompanies occupation of the  $1\pi_g^*$  orbital parallel to the surface. This results in an increased bond strength between peroxy oxygen and platinum surface, at the expense of the oxygen-oxygen bond strength.

The similarity of the static spectra for peroxy oxygen [Fig. 4(b)] and dissociated oxygen with our transient spectra from pump probe scans (Fig. 8) reveal two possibilities for the nature of the metastable oxygen state. It is either due to a transition of the excited superoxo ( $O_2^-$ ) into a transient (highly excited) dissociation state, or more likely a transition into an (excited) peroxy ( $O_2^{2-}$ ) state. These two possible processes are related—as the O-O bond in peroxy ( $O_2^{2-}$ ) oxygen is weakened it is referred to as a precursor state for dissociation.<sup>22,38</sup> We exclude the possibility that the transient state reflects desorption of molecular oxygen. A “reversible” replenished desorption is not possible: because significant refilling of the depleted oxygen sites within 1 ms (the repetition rate of the experiment) is negligible given the ambient pressure of  $10^{-10}$  torr. Experiments at higher fluences, where the surface is completely depleted by the laser pulse, show that diffusion on the surface from areas surrounding the laser spot does not occur.

A quantitative comparison of the peak height observed in the transient spectrum compared with the static spectrum for atomic oxygen can provide an estimate on the actual excitation rate of the oxygen molecules. Since the atomic oxygen layer on the Pt surface for both the TDS and the static UPS spectrum are prepared by temperature (photonic) heating, the oxygen coverage for both cases should be the same. Therefore, by comparing the signature peak intensity ratio of the peroxy transient spectrum and the atomic static spectrum, we can estimate the peroxy oxygen excitation rate. From the integrated peak intensities of our TDS spectra we find that 25% of the molecules of the original molecular saturation layer are dissociated. The peak intensities ratio for the peroxy transient spectrum and the atomic state spectrum is about 70%. Therefore we estimate the peroxy oxygen excitation rate is about 18%. At first glance this seems to be surprisingly high; however, even higher excitation rates of molecules due to femtosecond induced excitations have been reported before. For  $O_2/Pt(111)$ , for example, complete depletion of the surface by a single intense laser pulse has been reported<sup>29</sup> (there the fluence was several orders of magnitude higher than in our experiment).

The excitation mechanism of the adsorbate itself, the coupling of the excited electron gas and the adsorbate, can be described on a microscopic scale by means of direct electron (hole) transfer processes between the excited electron gas into the lowest unoccupied molecular orbital (LUMO) [high-

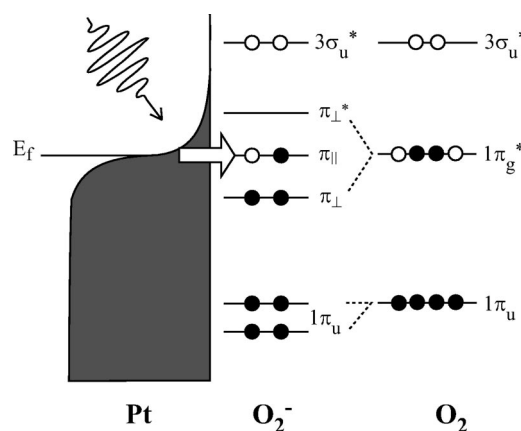


FIG. 11. The electron gas is rapidly heated up due to ultrafast pump pulse excitation. Due to an increased population above the Fermi level, electrons tunnel to the  $\pi_{\parallel}$  bond of the oxygen molecule.

est occupied molecular orbital (HOMO)] states of the adsorbate. A schematic of the expected molecular orbitals of superoxo and peroxy oxygen is shown in Fig. 11.<sup>29,39</sup> To account for femtosecond laser induced desorption processes on  $O_2/Pt(111)$ , it has been proposed that the substrate electrons couple to the unoccupied  $3\sigma_u^*$  level.<sup>30</sup> Furthermore, for  $O_2/Pd(111)$  hole transfer into the occupied part of the  $1\pi_g^*$  level has been suggested to be important.<sup>40</sup> In the present case, where a transformation from the superoxo into a peroxy state is the most likely mechanism, we propose an electron transfer from the platinum substrate to the unoccupied  $1\pi_g^*$  orbital of the superoxo state, which is oriented parallel to the surface. There are two justifications: (i) changes in the occupation of this level involve a charge transfer into the respective  $\pi$  orbital from the substrate to the adsorbate, corresponding to the different charge states of the two adsorption species;<sup>22</sup> and (ii) in the superoxo state, the  $\pi_{\parallel}$  orbital is only half filled and is therefore located at the Fermi level. This location would account for the observed high excitation probability, since the excited electron density in the substrate is highest at the Fermi level. Note, for example, that the  $3\sigma_u^*$  level of the oxygen lies  $\sim >1$  eV higher in energy, so that to efficiently populate this level, much higher electron temperatures and laser intensities are required.<sup>41</sup>

From this discussion, it is clear that the electronic excitation rate is highest for maximum substrate electron temperature, just a few tens of femtoseconds after the arrival of the pump pulse, and that it decreases as the electron gas cools. Therefore we conclude that the temporal delay of the transient adsorbate peak of about 500 fs with respect to time zero and the maximum in electron temperature, respectively, does not reflect the electronic excitation of the oxygen. It must arise from the change in chemical state accompanied by motion of the molecule itself. The local minimas (adsorption sites) of the corresponding potential energy surfaces for superoxo and peroxy oxygen define the general direction of this motion, from the bridge site to the hollow site [see Fig. 4(a)]. As discussed above, this involves a change in orientation (rotation) and bond length (vibration) within the mol-

ecule. The rise time of the signal can therefore be related to an effective coupling time  $\tau_e$  between the substrate electron gas and nuclear (not electronic) degrees of freedom, as typically introduced using a phenomenological frictional model for the description of substrate-adsorbate interaction.<sup>42</sup> Typical values of the coupling time  $\tau_e$  for direct energy exchange between the electron gas and the adsorbate lie in the range of a few 100 fs to several ps,<sup>9,43,44</sup> in agreement with our observations.

The decay of the signal from the  $1\pi_g^*$  level over several picoseconds can be interpreted as the actual lifetime of the metastable intermediate oxygen state. In case of a peroxo oxygen modification, this decay can occur via back charge transfer to the platinum substrate and/or energy exchange (thermalization) with electron gas and lattice. However, although decay back into the original ground state must be dominant under the present conditions, it is most likely not the only possible reaction channel. Different decays are also present in case of thermal excitation (see TDS), and have been observed previously for femtosecond laser excitation.<sup>9,43,44</sup> In these decay channels, the excited oxygen state has to be viewed as precursor to the new final state that was observed in real time by means of photoemission spectroscopy in our experiment. The permanent changes in the spectra over 1–2 h likely result from the cumulative effects of the secondary decay. As discussed above, peroxo oxygen tends to be the preferred adsorption site at low surface coverage, with a maximum peroxo-state population for about 0.3 monolayers of oxygen coverage.<sup>21</sup> Thus a possible explanation for the permanent, nontransient change in valence-band structure may be the result of desorption of oxygen over time and the consequent increase of the stable peroxo population. A buildup of atomic oxygen on the surface on long time

scales is a second possibility. It is unlikely that surface contamination from other species causes this permanent change, since the chamber is maintained in ultrahigh vacuum during the experiment and the contaminant is not likely to contribute to the 6-eV peak that we observe.

## V. CONCLUSION

We have demonstrated the use of ultrafast EUV pulses to directly monitor *different steps* in a hot-electron driven surface reaction on femtosecond time scales. We have shown that ultrafast charge-transfer processes between a Pt surface and adsorbed molecular oxygen can lead to a reversible chemical transformation on time scales as short as 0.5 ps. By monitoring both the characteristic valence-band photoemission spectrum, as well as the Fermi edge, we have shown that the hot nonequilibrium electron distribution relaxes before any change in bonding between the O<sub>2</sub> and Pt can occur. The lifetime of the observed metastable oxygen modification is of the order of several picoseconds. Ultrafast EUV photoelectron spectroscopy is a powerful technique, complementary to other techniques, for obtaining dynamic and local order information about a surface, on time scales relevant to the making and breaking of bonds in surface reactions.

## ACKNOWLEDGMENTS

The authors acknowledge support for the work from the National Science Foundation. The authors also thank D. Attwood at Lawrence Berkeley National Laboratory for fabricating the EUV multilayer mirrors used in this experiment.

\*Electronic address: clei@jila.colorado.edu

<sup>1</sup>*Laser Spectroscopy and Photochemistry on Metal Surfaces*, edited by H. L. Dai and W. Ho (World Scientific, Singapore, 1995).

<sup>2</sup>R. Cavanagh, D. King, J. Stephenson, and T. Heinz, *J. Phys. Chem.* **97**, 786 (1993).

<sup>3</sup>S. Backus, C. Durfee, M. Murnane, and H. Kapteyn, *Rev. Sci. Instrum.* **69**, 1207 (1998).

<sup>4</sup>P. Kratzer and M. Scheffler, *Comput. Sci. Eng.* **3**, 16 (2001).

<sup>5</sup>J.W. Gadzuk, *Chem. Phys.* **251**, 87 (2000).

<sup>6</sup>A. Zewail, *Ultrafast Dynamics of the Chemical Bond I and II* (World Scientific, Singapore, 1994).

<sup>7</sup>M. Bauer, C. Mathieu, S. Demokritov, B. Hillebrands, P. Kolodin, S. Sure, H. Dotsch, V. Grimalsky, Y. Rapoport, and A. Slavin, *Phys. Rev. B* **56**, R8483 (1997).

<sup>8</sup>H. Petek, M. Weida, H. Nagano, and S. Ogawa, *Science* **288**, 1402 (2000).

<sup>9</sup>T. Germer, J. Stephenson, E. Heilweil, and R. Cavanagh, *Phys. Rev. Lett.* **71**, 3327 (1993).

<sup>10</sup>M. Bonn, C. Hess, S. Funk, J. Miners, B. Persson, M. Wolf, and G. Ertl, *Phys. Rev. Lett.* **84**, 4653 (2000).

<sup>11</sup>S. Hüfner, *Photoelectron Spectroscopy* (Springer-Verlag, Berlin, 1995).

<sup>12</sup>H.J. Freund and N. Neumann, *Appl. Phys. A: Solids Surf.* **47**, 3 (1988).

<sup>13</sup>*Application of Synchrotron Radiation* edited by W. Eberhardt, Springer Series in Surface Science Vol. 35 (Springer-Verlag, Berlin, 1995), Chap. 3, pp. 65–126.

<sup>14</sup>U. Höfer, I.L. Shumay, C. Reu, U. Thomann, W. Wallauer, and T. Fauster, *Science* **277**, 1480 (1997).

<sup>15</sup>A. Rettenberger and R. Haight, *Phys. Rev. Lett.* **76**, 1912 (1996).

<sup>16</sup>A. Rundquist, C. Durfee, Z. Chang, C. Herne, S. Backus, M. Murnane, and H. Kapteyn, *Science* **280**, 1412 (1998).

<sup>17</sup>M. Bauer, C. Lei, K. Read, R. Tobey, J. Gland, M.M. Murnane, and H.C. Kapteyn, *Phys. Rev. Lett.* **87**, 025501 (2001).

<sup>18</sup>*Handbook of Optical Constants of Solids*, edited by E. D. Palik (Academic Press, New York, 1986).

<sup>19</sup>L. Nugent-Glandorf, M. Scheer, D. Samuels, V. Bierbaum, and S.R. Leone, *Rev. Sci. Instrum.* **73**, 1875 (2002).

<sup>20</sup>J. Gland, B. Sexton, and G. Fisher, *Surf. Sci.* **95**, 587 (1980).

<sup>21</sup>H. Steininger, S. Lehwald, and H. Ibach, *Surf. Sci.* **123**, 1 (1982).

<sup>22</sup>A. Eichler and J. Hafner, *Phys. Rev. Lett.* **79**, 4481 (1997).

<sup>23</sup>B. Stipe, M. Rezaei, W. Ho, S. Gao, M. Persson, and B. Lundqvist, *Phys. Rev. Lett.* **78**, 4410 (1997).

<sup>24</sup>C. Puglia, A. Nilsson, B. Hernnas, O. Karis, P. Bennich, and N. Martensson, *Surf. Sci.* **342**, 119 (1995).

<sup>25</sup>F.J. Kao, D.G. Busch, D.G.d. Costa, and W. Ho, *Phys. Rev. Lett.* **70**, 4098 (1993).

<sup>26</sup>W. Eberhardt, T. Upton, S. Cramm, and L. Incoccia, *Chem. Phys. Lett.* **146**, 561 (1988).

- <sup>27</sup>A. Eichler, F. Mittendorfer, and J. Hafner, *Phys. Rev. B* **62**, 4744 (2000).
- <sup>28</sup>M.L. Bocquet, J. Cerd, and P. Sautet, *Phys. Rev. B* **59**, 15 437 (1999).
- <sup>29</sup>S. Deliwala, R. Finlay, J. Goldman, T. Her, W. Mieher, and E. Mazur, *Chem. Phys. Lett.* **242**, 617 (1995).
- <sup>30</sup>R.J. Finlay, T.H. Her, C. Wu, and E. Mazur, *Chem. Phys. Lett.* **274**, 499 (1997).
- <sup>31</sup>NIST Standard Reference Database 71 “NIST Electron Inelastic-Mean-Free-Path Database,” Version 1.1, Gaithersburg, 2000.
- <sup>32</sup>W. Fann, R. Storz, H. Tom, and J. Bokor, *Phys. Rev. Lett.* **68**, 2834 (1992).
- <sup>33</sup>P. Siffalovic, M. Drescher, M. Spieweck, T. Wiesenthal, Y.C. Lim, R. Weidner, A. Elizarov, and U. Heinzmann, *Rev. Sci. Instrum.* **72**, 30 (2001).
- <sup>34</sup>E. Zarate, P. Apell, and P.M. Echenique, *Phys. Rev. B* **60**, 2326 (1999).
- <sup>35</sup>R. Knorren, K.H. Bennemann, R. Burgermeister, and M. Aeschli-  
mann, *Phys. Rev. B* **61**, 9427 (2000).
- <sup>36</sup>S.I. Anisimov, B.L. Kapeliovich, and T.L. Perelman, *Zh. Eksp.  
Teor. Fiz.* **66**, 776 (1974) [*Sov. Phys. JETP* **66**, 776 (1974)].
- <sup>37</sup>B. Rethfeld (private communication).
- <sup>38</sup>P.D. Nolan, B.R. Lutz, P.L. Tanaka, J.E. Davis, and C.B. Mullins,  
*J. Chem. Phys.* **111**, 3696 (1999).
- <sup>39</sup>I. Panas and P. Siegbahn, *Chem. Phys. Lett.* **153**, 458 (1988).
- <sup>40</sup>J. Misewich, S. Nakabayashi, P. Weigand, M. Wolf, and T. Heinz,  
*Surf. Sci.* **363**, 204 (1996).
- <sup>41</sup>W.D. Mieher and W. Ho, *J. Chem. Phys.* **99**, 9279 (1993).
- <sup>42</sup>F. Budde, T.F. Heinz, A. Kalamarides, M.M.T. Loy, and J.A. Mis-  
ewich, *Surf. Sci.* **283**, 143 (1993).
- <sup>43</sup>M. Bonn, S. Funk, C. Hess, D. Denzler, C. Stampfl, M. Scheffler,  
M. Wolf, and G. Ertl, *Science* **285**, 1042 (1999).
- <sup>44</sup>L.M. Struck, L.J. Richter, S.A. Buntin, R.R. Cavanagh, and J.C.  
Stephenson, *Phys. Rev. Lett.* **77**, 4576 (1993).